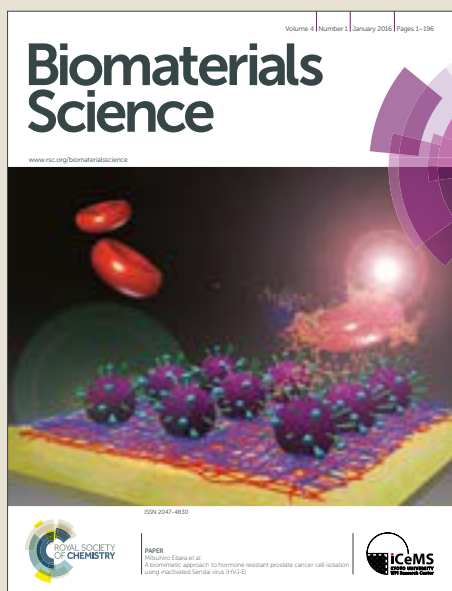


# Biomaterials Science

Accepted Manuscript



This article can be cited before page numbers have been issued, to do this please use: Y. Li, X. Wang, J. Yan, Y. Liu, R. Yang, D. Pan, L. Wang, Y. Xu, X. Li and M. Yang, *Biomater. Sci.*, 2019, DOI: 10.1039/C9BM00653B.



This is an Accepted Manuscript, which has been through the Royal Society of Chemistry peer review process and has been accepted for publication.

Accepted Manuscripts are published online shortly after acceptance, before technical editing, formatting and proof reading. Using this free service, authors can make their results available to the community, in citable form, before we publish the edited article. We will replace this Accepted Manuscript with the edited and formatted Advance Article as soon as it is available.

You can find more information about Accepted Manuscripts in the [author guidelines](#).

Please note that technical editing may introduce minor changes to the text and/or graphics, which may alter content. The journal's standard [Terms & Conditions](#) and the ethical guidelines, outlined in our [author and reviewer resource centre](#), still apply. In no event shall the Royal Society of Chemistry be held responsible for any errors or omissions in this Accepted Manuscript or any consequences arising from the use of any information it contains.

# Nanoparticle Ferritin-bound Erastin and Rapamycin: A Nanodrug Combined Autophagy and Ferroptosis for Anticancer Therapy

Yaoqi Li,<sup>a‡</sup> Xinyu Wang,<sup>a,b‡</sup> Junjie Yan,<sup>b</sup> Yu Liu,<sup>b</sup> Runlin Yang,<sup>b</sup> Donghui Pan,<sup>b</sup> Lizhen Wang,<sup>b</sup> Yuping Xu,<sup>b</sup> Xiaotian Li,<sup>a</sup> Min Yang<sup>a,b</sup>

Received 00th January 20xx,  
Accepted 00th January 20xx

DOI: 10.1039/x0xx00000x

www.rsc.org/

Ferroptosis and autophagy are two forms of regulation of cell death that play important role in cancer therapy. However, little is known about the combination therapeutic effect of ferroptosis and autophagy in cancer therapy. Here, in this study, we constructed a novel carrier-free nanodrug called nanoparticle ferritin-bound erastin and rapamycin (NFER). NFER nanodrug was prepared by emulsification technique with an average size of 78.8 nm and zeta potential of  $-25.9 \pm 3.3$  mV. The controllable drug encapsulation efficiency and loading ratios in NFER can be obtained. This nanodrug showed high stability both in water and PBS for several days. Release studies demonstrated that rapamycin and erastin would reach equilibrium after 24 h and 36 h respectively, and maximum of released percentages both reached beyond 30%. In vitro study revealed that the NFER show robust ferroptosis inducing capability by downregulation of glutathione peroxidase-4 (GPX4) and lipid peroxidation accumulation. The autophagy process induced by rapamycin in NFER also plays an important role in strengthening ferroptosis. The selectively cancer cell killing ability of NFER was verified in cancer cells and normal cells. The ferroptosis-induced cytotoxicity was confirmed by several ferroptosis and autophagy inhibitors. Furthermore, NFER nanodrug showed improved control of tumor recurrence in the 4T1 tumor resection model. In summary, these results demonstrated NFER exhibits excellent properties as a nanodrug and the cell death induced by NFER was through autophagy-associated ferroptosis pathway. This study based on protein nanodrug induced autophagy-associated ferroptosis would provide a new insight into cancer therapy.

## Introduction

Cell death, which plays an important role in cancer therapy, have multiple forms including necrosis, apoptosis, necroptosis, autophagy, and ferroptosis.<sup>1, 2</sup> Conventional cancer chemotherapy is primarily directed to inducing apoptosis.<sup>3</sup> However, it has been determined that many cancer cells are chemo-resistant and have defects in the induction of apoptosis.<sup>4</sup> Ferroptosis, an iron- and reactive oxygen species (ROS)-dependent form of cell death, has been proved to be effective in killing cancer cells, especially for those expressing oncogenic RAS.<sup>5, 6</sup>

Nanomedicine has been widely explored for effective cancer imaging and targeted cancer therapy.<sup>7</sup> Varieties of iron based nanoparticles have been used in ferroptosis-based cancer treatment, such as iron oxide nanoparticles,<sup>8, 9</sup> amorphous iron nanoparticles,<sup>10</sup>

iron-organic network nanoparticles,<sup>11, 12</sup> FeGd nanoparticles,<sup>13</sup> and FePt nanoparticles.<sup>14</sup> The iron can be released in the acidic lysosome as  $\text{Fe}^{2+}$  or  $\text{Fe}^{3+}$  ions, which can produce ROS and induce lipid peroxidation by Fenton reaction.<sup>15, 16</sup> Although ferroptosis can be induced by these iron-based inorganic or organic nanomaterials in vivo, high dose iron are always needed without another agent (beyond iron) that contributes to the ferroptosis. And this may be a concern about the biosafety for applying these nanomaterials for further clinical translation.

Protein is one of the most promising drug carriers, which have attracted numerous attentions in cancer therapy.<sup>17-19</sup> A variety of proteins have been used as drug carriers, including albumin<sup>20</sup>, ferritin,<sup>21, 22</sup> lactoferrin,<sup>23</sup> silk fibroin,<sup>24</sup> etc. Abraxane, the first albumin-bound drug delivery system approved by FDA in oncology, is a nanoparticle albumin-bound form of paclitaxel.<sup>25</sup> The success of Abraxane inspired a large number of researches in drug delivery using protein carrier.<sup>26, 27</sup> Ferritin is a universal intracellular protein that stores and releases iron in a controlled manner, which can also be found in serum.<sup>28</sup> It acts as a buffer against iron deficiency and iron overload in human body.<sup>29</sup> The high targeting efficiency for transferrin receptor 1 made it an ideal drug carrier for imaging and treatment of several types of cancer, including colon cancer, liver cancer, and ovarian cancer.<sup>30, 31</sup> Recently, ferritin was reported that it can induce ferroptosis when it is intracellular degraded by autophagy

<sup>a</sup> School of Pharmaceutical Sciences, Zhengzhou University, Zhengzhou 450001, China. E-mail: lixi@zzu.edu.cn;

<sup>b</sup> Key Laboratory of Nuclear Medicine, Ministry of Health, Jiangsu Key Laboratory of Molecular Nuclear Medicine, Jiangsu Institute of Nuclear Medicine, Wuxi, 214063, China. E-mail: wangxinyu@jsnm.org; yangmin@jsnm.org

† Electronic supplementary information (ESI) available. See DOI: 10.1039/x0xx00000x

‡ These authors contributed equally to this work.

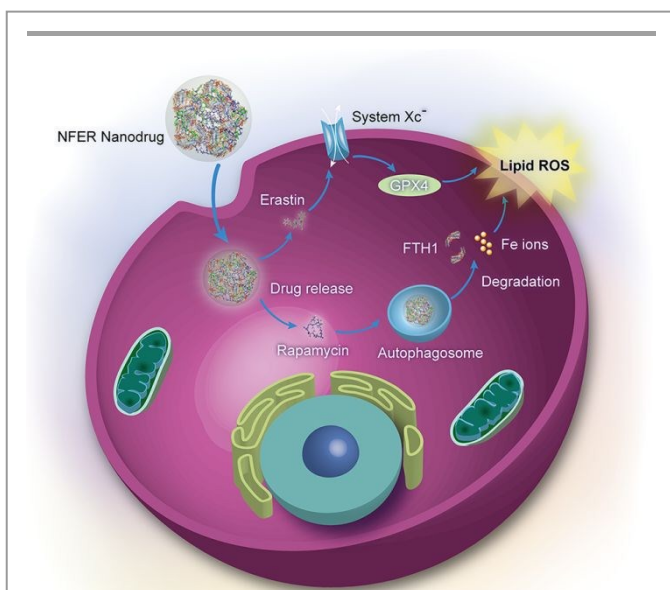


**Fig.1** Schematic illustration of intracellular autophagy-mediated ferroptosis induction process by NFER nanodrug. The released erastin will inhibit cysteine uptake by system  $Xc^-$  and then induce ferroptosis by downregulation of GPX4. At the same time, the released rapamycin will induce the autophagy process. The degradation of ferritin in autophagosome will lead to the release of Fe ions, which enhance the ferroptosis process by accumulation of Lipid ROS.

process,<sup>32, 33</sup> which is an evolutionarily conserved lysosomal degradation pathway that removes damaged organelles and protein aggregates from the cytoplasm.<sup>34</sup>

In the present study, we prepared an Abraxane-inspired nanodrug named nanoparticle ferritin-bound erastin and rapamycin (NFER) which consists of iron-abundant protein ferritin, erastin, and rapamycin. Erastin, an oncogenic RAS-selective lethal small molecule, has been used as a typical ferroptosis activator.<sup>35, 36</sup> Rapamycin, also known as sirolimus, is an FDA-approved immunosuppressive and cardiology drug.<sup>37</sup> It is also a well-known autophagy inducer.<sup>38</sup> The NFER nanodrug based on ferritin, erastin, and rapamycin was fabricated using emulsification technique without additional carrier. This carrier-free nanodrug was designed to induce both autophagy and ferroptosis. Furthermore, since autophagy process can degrade the ferritin as reported,<sup>32</sup> the ferroptosis effect may be enhanced after that. This autophagy-mediated ferroptosis induction process in cells by NFER was shown in Fig. 1.

## Experimental Section

**Materials.** Rapamycin was purchased from Arkpharminc (Shanghai, China). Erastin was obtained from MedChem Express (Shanghai, China). Ferritin from equine spleen and Pluronic F-127 were purchased from Sigma Aldrich (Shanghai, China). Deferoxamine was obtained from Novartis (Shanghai, China), Glutathione reduced form (GSH) was purchased from Tokyo Chemical Industry (Shanghai, China). 3BDO was purchased from

Selleck (Shanghai, China). Float-A-Lyzer G2 Dialysis Cassettes (MWCO 3.5 kDa) and Tube-O-DIALYZER™ Micro Dialysis System (MWCO 50 kDa) were purchased from Sangon Biotech (Shanghai, China). C11-BODIPY was obtained from Thermo Fisher. Cy5.5 NHS ester (non-sulfonated) was purchased from ApexBio Technology. The kits for MTT cell proliferation and cytotoxicity assay, enhanced BCA protein assay, and reactive oxygen species assay, Hoechst 33342 staining solution for live cells, anti-LC3B, anti-GPX4, anti-Atg-7, and anti-Actin were purchased from Beyotime Institute of Biotechnology (Jiangsu, China). Anti-ferritin heavy chain (FTH1) purchased from GeneTex were used as primary antibodies. Goat anti-rabbit IgG (H+L)-HRP conjugate and goat anti-mouse IgG (H+L)-HRP conjugate obtained from Beyotime were used as secondary antibodies. All obtained chemicals were used without further purification.

**Preparation of NFER nanodrug.** NFER nanodrug was prepared using emulsification technique. Rapamycin and erastin stock solutions were dissolved in a proper amount of dichloromethane respectively, they were then mixed according to various drug/protein ratios as the oil phase (see Table S1, ESI<sup>†</sup>). Ferritin (50 mg/mL) was dissolved in PBS to a final concentration of 1 mg/mL as the aqueous phase. The volume ratio of the aqueous phase to the oil phase is 1:1. The aqueous phase was added to the oil phase, which led to the formation of a two-phase liquid mixture, and then the emulsions were sonicated in a mechanical sonicator for 10 min. The resulting emulsion was then placed in dialysis tubing, dialyzed 8 times in DI water which was replaced by fresh water every 2 h. 2% (w/v) PEG 300 (a lyoprotectant) was then added to the dialyzed solution. After lyophilization for 36 h, it was dissolved in sterile water to obtain the final nanodrug concentrated solution. Drug loading efficiency and encapsulation efficiency were calculated as follows:  $Drug\ loading\ efficiency\ (\%) = (Weight\ of\ the\ drug\ in\ NFER\ nanodrug) / (Weight\ of\ the\ NFER\ nanodrug) * 100\%$ ;  $Encapsulation\ efficiency\ (\%) = (Weight\ of\ the\ drug\ in\ NFER\ nanodrug) / (Weight\ of\ the\ feeding\ drug) * 100\%$ . The concentration of NFER was determined by lyophilization and weight of NFER solution without PEG.

**Characterization.** Morphology of the prepared nanodrug was examined on a Tecnai G2-20 instrument operated at 200 kV for transmission electron microscopy (TEM) images. The size distribution and zeta potential of the nanodrug were measured by dynamic light scattering (DLS) using a Zetasizer Nano ZSE (Malvern Instruments, Ltd.). An Agilent Cary 60 UV-vis spectrophotometer was used to measure UV-vis absorption of the sample solutions. The contents of Fe in NFER and ferritin were detected by ICP-MS (Agilent 7700X, USA). High-performance liquid chromatography (HPLC) was performed with Waters 1525 equipped with 2998 photodiode array detector to detect the drug loading content and encapsulation efficiency.

**Stability study.** To investigate the in vitro stability of NFER, the concentrated solutions were mixed with PBS (pH 7.4) and water for 48 h, respectively, and were evaluated by measuring the hydrodynamic radius of the nanodrug by DLS every 12 h.

**In vitro release of rapamycin and erastin.** The concentrated NFER solution was dispersed in a dialysis tube (MWCO 50 kDa) containing 3 mL of PBS (pH 7.4) and was placed in a beaker containing 50 mL of buffer under magnetic stirring for 48 h. 200  $\mu$ L

of the external solution was taken out and the same volume of fresh PBS was added at different set times. The rapamycin and erastin released in the supernatant were detected by HPLC method.

For HPLC analysis, the flow rate was 0.1 mL/min, and the mobile phase consisted of 90% solvent A (acetonitrile) and 10% solvent B (pure water with 0.1% HAc) for rapamycin, and 50% solvent A (acetonitrile) and 50% solvent B (pure water with 0.1% HAc) for erastin. The detection was performed by UV-vis absorption at 278 nm.

**Cell culture.** PC12 cells (rat adrenal medulla cell line), 4T1 cells (mouse breast cancer cell line), and L929 cells from mouse fibroblast cell line were obtained from the Cell Bank in Shanghai Institute of Cell Biology, China. The cells were cultured in RPMI-1640 medium supplemented with 10% fetal bovine serum and 0.1% penicillin-streptomycin. Then they were cultured in a humidified atmosphere of a 37°C incubator with 5% CO<sub>2</sub>.

**In vitro cell viability assay.** MTT assay were employed to analyze the in vitro cell viability of rapamycin, erastin, ferritin, and NFER nanodrug. Briefly, cells were seeded in 96-well plates with the cell density of  $6 \times 10^3$  cells per well and incubated overnight. Then the drugs with different concentrations were added into the wells and incubated for 24 h. After that, the standard MTT assay was carried out to determine the cell viability.

To validate the NFER nanodrug-mediated cell death pathways, we selected several representative cell death inhibitors for cell viability assays, including such as desferrioxamine mesyllate (DFO, ferroptosis inhibitors), GSH and 3BDO (autophagy inhibitor).<sup>39</sup> The cells were incubated with each type of inhibitors and NFER nanodrug for 24 h. The concentrations of the inhibitors were used as follows: DFO, 50 μM; GSH, 5 mM; 3BDO, 60 μM. After the treatment, cell viabilities were assessed using the MTT assay.

**Cell staining for fluorescence microscopy.** PC12 cells were seeded with a density of  $5 \times 10^5$  per well in 6-well plates and incubated overnight. Cells were treated with several different concentrations of NFER and then allow for further incubation. After incubation for 24 h, the culture medium was replaced and then washing by PBS for three times. 2.5 mL of fresh medium containing the nuclear dye Hoechst 33342 were added into the wells and incubated for 30 min. After that, cells were washed by PBS for three times, then the lipid peroxidation sensor C11-BODIPY was added into each well with the final concentration of 5 μM and incubated for another 30 min. After washing by PBS, the cells were observed using a fluorescence microscopy (Olympus). The fluorescence intensity of C11-BODIPY were also analyzed by flow cytometry.

**ROS detection in vitro.** Intracellular ROS changes were detected by loading the fluorescent probe DCFH-DA. PC12 cells were seeded with a density of  $5 \times 10^5$  per well in 6-well plates overnight after incubated with several different concentration of nanodrug and 10 μM H<sub>2</sub>O<sub>2</sub> for 24 h. DCFH-DA with a final concentration of 10 μM was mixed with the fresh cell culture medium and added into wells. The cells were incubated in a 37°C incubator for 20 min. After that, the cells were washed three times by PBS. Finally, cells were digested and dispersed in 500 μL PBS for flow cytometry study.

**Western blot analysis.** The samples were lysed. Cell lysates were prepared in Western and IP lysis buffer containing 20 mM Tris (pH

7.5), 150 mM NaCl, 1% Triton X-100, sodium pyrophosphate, β-glycerophosphate, EDTA, Na<sub>3</sub>VO<sub>4</sub>, leupeptin, and other inhibitors. Protein levels were quantified using the enhanced BCA protein assay kit. The protein samples were run on 4–12% Tris-glycine gels (Invitrogen Novex) and transferred to a polyvinylidene fluoride (PVDF) membranes and then incubated overnight with primary antibodies as follows: anti-GPX4 (1:15000), anti-LC3B (1:200), anti-Atg-7 (1:1000), anti-Ferritin Heavy Chain (1:500), and anti-Actin (1: 1000). The samples were then incubated with horseradish peroxidase-linked secondary antibodies. The relative quantity of proteins was analyzed by Quantity one software and normalized to that of loading controls.

**Hemolysis assay.** The method used for hemolysis assay is based on the previous study.<sup>40</sup> All animal experiments were conducted following the National Institutes of Health guidelines for the care and use of laboratory animals and approved by the Institutional Animal Care and Ethics Committee of Jiangsu Institute of Nuclear Medicine (Wuxi, China). For the hemolysis ratio test, blood drawn from mice was placed in a blood anticoagulant tube containing heparin. The serum was removed from the blood by centrifugation at 2000 rpm for 5 min to obtain red blood cells (RBCs) and washed three times with PBS. The centrifuged RBCs were diluted to a concentration of 2% suspension with PBS. Every test sample was incubated with 2% suspension at 37°C for 1 h. Negative and positive controls were selected from PBS and DI water, respectively. Finally, the solutions were centrifuged at 2000 rpm for 5 min, and 200 μL of the supernatant was transferred to a 96-well plate. The absorbance at 545 nm were measured using a microplate reader (BioTek, uQuant, USA). The hemolysis ratios (%) were calculated as follows:  $(A_{\text{sample}} - A_{\text{negative control}}) / (A_{\text{positive control}} - A_{\text{negative control}}) \times 100$ , where  $A_{\text{sample}}$ ,  $A_{\text{negative control}}$ , and  $A_{\text{positive control}}$  represented absorbances of samples, negative and positive controls, respectively.

**Preparation of NFER@F127 and F+E+R@F127.** NFER group: NFER and F127 with a mass fraction of 20% were prepared by mixing in a volume ratio of 1:2 to form NFER@F127; F+E+R group: Take the corresponding volume of ferritin, rapamycin, and erastin according to the mass contained in each component of NFER. The mixed solution was thoroughly prepared by mixing F127 with a mass fraction of 20% at a volume ratio of 1:2 to form F+E+R@F127. NFER@F127 and F+E+R@F127 will form a hydrogel when the temperature increased to 37°C.

**In vivo experiments.** All animal experiments were conducted following the National Institutes of Health guidelines for the care and use of laboratory animals and approved by the Institutional Animal Care and Ethics Committee of Jiangsu Institute of Nuclear Medicine (Wuxi, China). Female BALB/c nude mice (4–6 weeks) were purchased from Changzhou Cavans Company, Jiangsu Province. The method used for in vivo experiment is based on the previous study<sup>41</sup>. For the construction of the tumor model, 4T1 cells ( $5 \times 10^6$ ) suspended in PBS were subcutaneously injected into the right hip of each female BALB/c nude mice. When the tumor grows to about 100 mm<sup>3</sup> (about 6–7 days), nude mice were randomly divided into three groups (n = 5) and anesthetized (the nude mice are anesthetized with isoflurane, the anesthesia is maintained through the nasal cavity during the operation), and about 99% of the tumors are removed using a sterile instrument, 1% of the tumor was left to

simulate microscopic tumors remaining after surgery. NFER@F127, F+E+R@F127 were injected into the surgical site immediately after the operation (The dose was rapamycin equivalent 0.2 mg/kg), and each nude mouse was injected with approximately 120  $\mu\text{L}$  of mixed gel drug and sutured by sterile surgery. Intramuscular injection of penicillin for 3 days in nude mice. The body weight and tumor size of nude mice were monitored daily, the tumor volume was calculated according to the following formula:  $\text{width}^2 \times \text{length} \times 0.5$ .

**Statistical analysis.** All data were generated with at least three independent experiments. Each experiment in the cell death analysis was carried out by 3-6 replicates. Data were analyzed using Student's t-test, and represented as means  $\pm$  s.d. ( $n \geq 3$ ). Differences with a P value less than 0.05 was deemed significant. All statistical analyses were performed by GraphPad Prism 7 (GraphPad Software).

## Results and Discussion

**Fabrication and characterization of NFER nanodrug.** NFER nanodrug was prepared by emulsification technique (Fig. 2A), which is often used for protein nanoparticles preparation.<sup>18, 42</sup> We also prepared this nanoparticle by self-assembly in PBS. However, the drug encapsulation efficiency is much lower than that of emulsification (Fig. S1, ESI †). For emulsification, erastin and rapamycin were dissolved in dichloromethane while the ferritin was in PBS. As erastin and rapamycin are both hydrophobic drugs, they can form hydrophobic center together with protein in emulsification process. The hydrodynamic diameter of NFER characterized by dynamic light scattering (DLS) was approximately 78 nm, which is almost 7-fold bigger than that of ferritin (Fig. 2B). The transmission electron microscopy (TEM) image showed that NFER had a sphere-like shape and a uniform size around 40 nm (Fig. 2C). Zeta potential measurements revealed a single population of both NFER and ferritin. The zeta potential of NFER is  $-25.9 \pm 3.3$  mV, while the value of ferritin is  $-7.01 \pm 3.29$  mV (Fig. 2D). The negative surface charge of NFER would contribute to their shielded transport in bloodstream and stability in solution. The UV-Vis spectra showed that the absorbance of NFER between 350-800 nm increased obviously compared with ferritin, which may attributed by the stronger light scattering of nanoparticles rather than protein (Fig. 2E). The iron contents in NFER and ferritin were measured by inductively coupled plasma mass spectrometry (ICP-MS). As shown in Fig. 2F, the iron content of NFER is 2.47 mg/kg, which is very close to that of ferritin. This can be explained by the low drug-loading ratio, which will be discussed further. And this may reveal that the emulsification fabrication process will not affect the iron content of ferritin in NFER nanodrug. The stability of NFER was further investigated by DLS. Interestingly, there was no significant change of the particle size observed for 2 days both in water and PBS buffer while it increased slightly in cell culture medium (Fig. 2G). These results revealed NFER have good stability. In summary, well-defined nanosized ferritin-based nanodrug were prepared for further evaluation.

**Drug loading and release.** Drug loading ability of NFER was investigated by emulsification of ferritin, erastin, and rapamycin with different ratios and analyzed by high-performance liquid chromatography (HPLC). The concentration of ferritin was set as 1

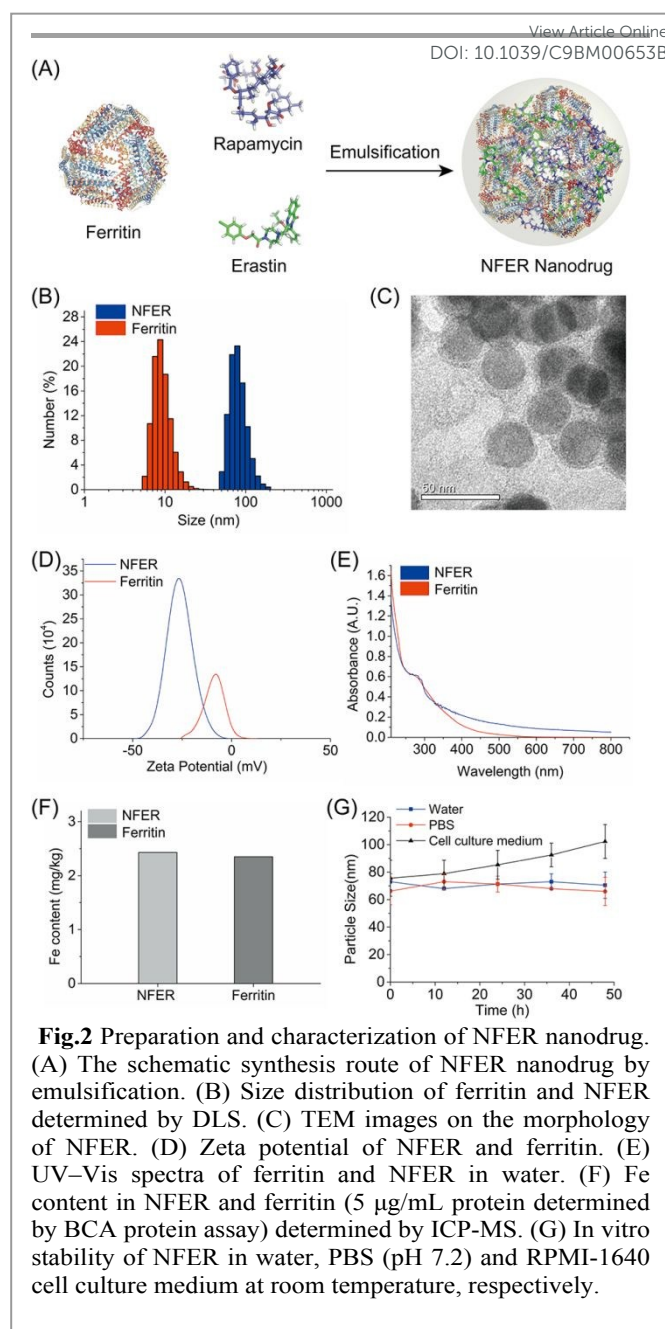
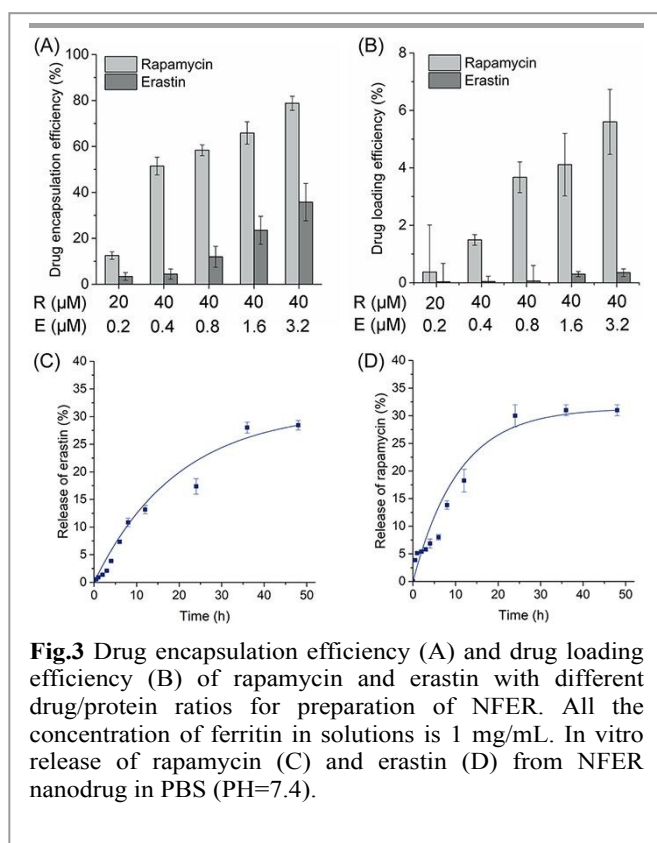


**Fig.2** Preparation and characterization of NFER nanodrug. (A) The schematic synthesis route of NFER nanodrug by emulsification. (B) Size distribution of ferritin and NFER determined by DLS. (C) TEM images on the morphology of NFER. (D) Zeta potential of NFER and ferritin. (E) UV-Vis spectra of ferritin and NFER in water. (F) Fe content in NFER and ferritin (5  $\mu\text{g}/\text{mL}$  protein determined by BCA protein assay) determined by ICP-MS. (G) In vitro stability of NFER in water, PBS (pH 7.2) and RPMI-1640 cell culture medium at room temperature, respectively.

mg/mL in PBS. As shown in in Fig. 3A and 3B, both drug encapsulation efficiency and drug-loading efficiency increased with increasing the erastin and rapamycin concentration in emulsion. The highest drug-loading ratios for erastin and rapamycin are 0.35% and 5.6%, while the highest drug encapsulation efficiency are 35.75% and 78.78%, respectively.

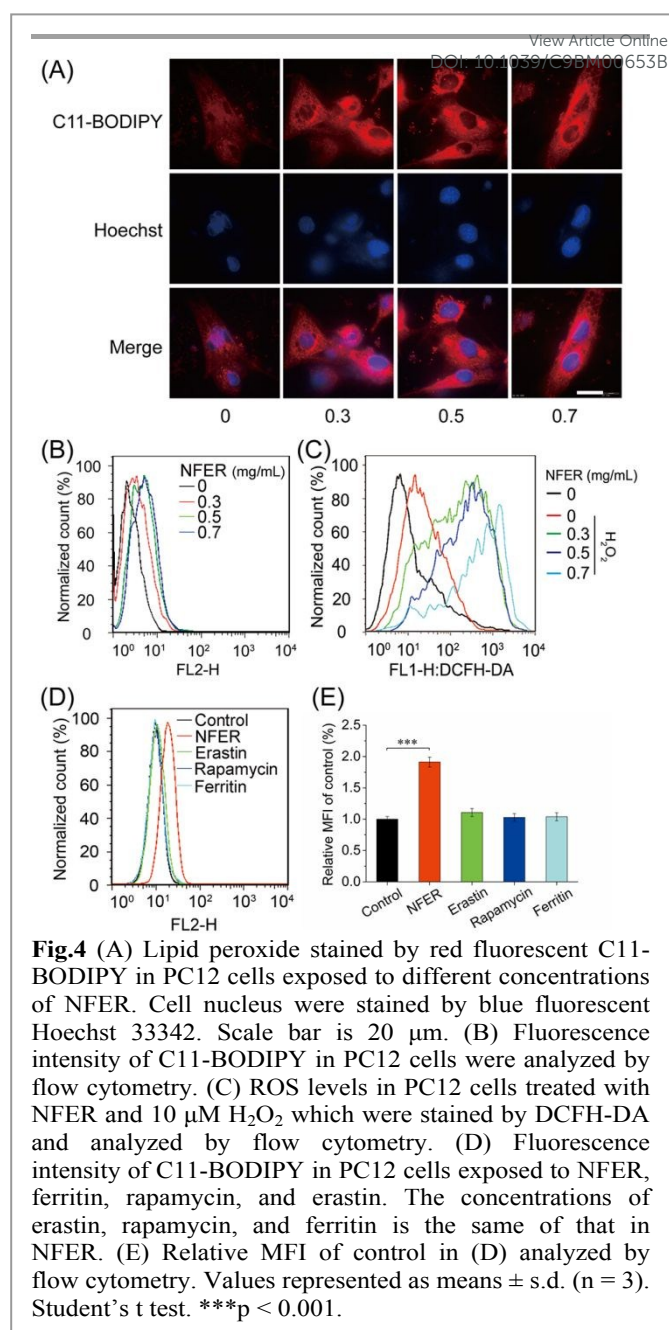
The release behavior of erastin and rapamycin in NFER was investigated by dialysis in PBS buffer (pH 7.4) for 48 h. As shown in Fig. 3C and 3D, both erastin and rapamycin was released faster in the first 24 h rather than the left time. The release curve of rapamycin became stable after 24 h, while erastin reached equilibrium after 36 h. In the end at 48 h, the accumulative release percentage of both two drugs can reach approximately 30%. As the nanoparticle kept stable in PBS for 48 h, it is reasonable for that the left 70% erastin and rapamycin in NFER was not released. The left



drug may be released until disassembly of the nanoparticles.

**NFER induced ferroptosis and autophagy in vitro.** Intracellular lipid peroxide (LPO) level is an important hallmark of ferroptosis,<sup>43, 44</sup> which was investigated by NFER nanodrug treatment. To verify the ferroptosis induction activity of NFER, intracellular LPO level was detected by fluorescence microscopy and flow cytometer. C11-BODIPY, a lipid peroxidation sensor,<sup>33</sup> was used to evaluate the LPO level in PC-12 cells (rat pheochromocytoma cell line). As shown in **Fig. 4A**, the cells treated with NFER showed much stronger fluorescence intensity rather than untreated cells. In addition, the fluorescence intensity was increased as the concentration of NFER increased. The fluorescence intensity was further verified by flow cytometer. The highest fluorescence intensity is 2.26-fold bigger than that of control, which was shown in **Fig. 4B** and **Fig. S2** (ESI †). Previous studies demonstrated that erastin can induce iron-dependent ferroptosis mediated by lipid peroxidation and ROS.<sup>5, 45</sup> Thus, to determine the intracellular oxidative stress after post-treatment, dichlorofluorescein diacetate (DCFH-DA) staining assay was performed. The cells were incubated with NFER and additional 10 µM H<sub>2</sub>O<sub>2</sub> to simulate the oxidative stress in tumor microenvironment. The oxidative stress enhancing ability of NFER was proved in **Fig. 4C** and **Fig. S2** (ESI †). The ferroptosis-inducing activity of NFER was compared with the three drugs alone by measuring the intracellular LPO levels. As shown in **Fig. 4D** and **4E**, cells treated with NFER showed significant increasing LPO level compared to the control group, while there is no obvious difference between the drugs alone. Overall, these results indicate that NFER have the strongest LPO inducing capability which is essential to ferroptosis.

Moreover, the protein level was determined to study the



ferroptosis and autophagy induced by NFER. Autophagy-related gene 7 (Atg-7) is one of the Atg genes, which is essential for conventional autophagic vacuole formation.<sup>46</sup> As shown in **Fig. 5A** and **5B**, Atg-7 increased obviously after NFER treatment. The highest Atg-7 level increased approximately 8 times compared with control. However, the cells treated with erastin or ferritin alone will not increase the Atg-7 level (**Fig. 5C** and **5D**). Microtubule-associated protein light chain 3 (LC3), a mammalian homolog of yeast Atg8, has been used as a specific marker to monitor autophagy.<sup>47</sup> Upon autophagy, lipidated LC3 protein tends to localize on the surface of autophagosome membranes, followed by a molecular form conversion from LC3-I form to LC3-II form.<sup>47, 48</sup> From the data in **Fig. 5A** and **5B**, it is apparently that the LC3II/LC3I ratio in 0.5 mg/mL NFER treated cells increased approximately 5-fold than control. Taken the results of Atg-7 and LC3II/LC3I protein

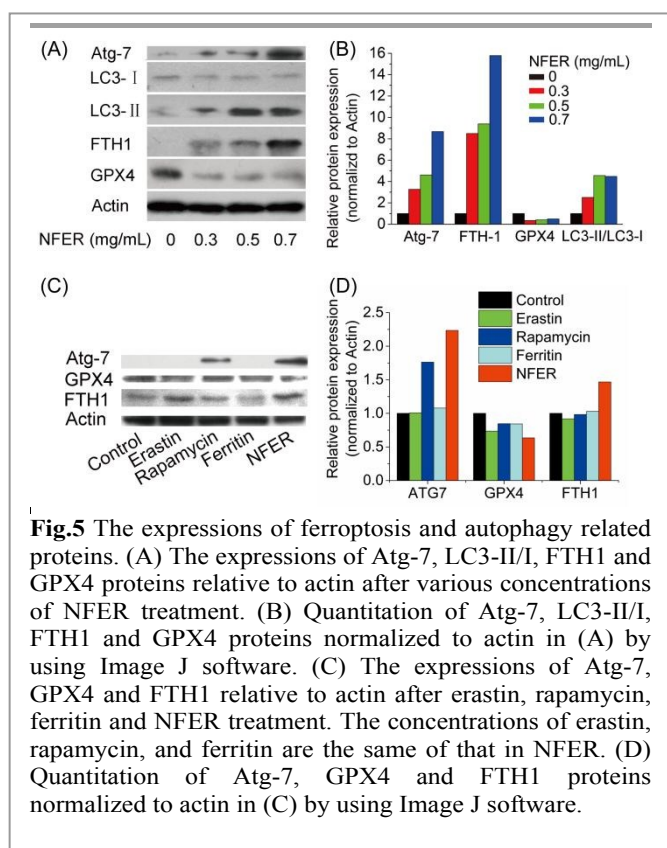


**Fig.5** The expressions of ferroptosis and autophagy related proteins. (A) The expressions of Atg-7, LC3-II/I, FTH1 and GPX4 proteins relative to actin after various concentrations of NFER treatment. (B) Quantitation of Atg-7, LC3-II/I, FTH1 and GPX4 proteins normalized to actin in (A) by using Image J software. (C) The expressions of Atg-7, GPX4 and FTH1 relative to actin after erastin, rapamycin, ferritin and NFER treatment. The concentrations of erastin, rapamycin, and ferritin are the same of that in NFER. (D) Quantitation of Atg-7, GPX4 and FTH1 proteins normalized to actin in (C) by using Image J software.

expressions together, we found that NFER have a remarkable autophagy inducing capability. Ferritin heavy polypeptide 1 (FTH1) is the component of ferritin which can be increased in cells after autophagy induced ferritin degradation.<sup>32</sup> As the autophagy process activated by NFER, FTH1 increased apparently (Fig. 5A and 5B), while the drugs alone could not induce the increasing of FTH1 (Fig. 5C and 5D). GPX4 is an antioxidant enzyme which plays an important role in inhibiting ferroptosis.<sup>2</sup> The GPX4 level decrease more than 60% compared with control after 0.7 mg/mL NFER treatment, which is very important for the accumulation of LPO. Furthermore, the protein expression of PC12 cells treated with NFER was also compared with two of the three drugs. As shown in Fig. S3 (ESI<sup>†</sup>), the highest Atg-7 level and lowest GPX4 level were achieved by NFER treatment compared to ferritin plus erastin, ferritin plus rapamycin or erastin plus rapamycin. Combined all these results, the NFER induced ferroptosis was confirmed by the downregulation of GPX4 and increasing of LPO level.

**In vitro ferroptosis induced cell death by NFER.** Before the study on the ferroptosis induced cell death, the cytotoxicity of ferritin, erastin, and rapamycin was evaluated in PC12 cells first. The drug concentrations for half reduce of cell viability (IC<sub>50</sub>) were 3.73, 0.37, 16.25  $\mu$ M for ferritin, erastin, and rapamycin, respectively (Fig. 6A). And the mass concentrations for IC<sub>50</sub> were 1.64, 0.0002, 0.015 mg/mL for ferritin, erastin, and rapamycin, respectively. And then the cytotoxicity of two drugs mixed with ferritin, erastin, rapamycin and a mixture of three drugs were evaluated in PC12 cells (Fig. S4, ESI<sup>†</sup>). It can be found that the combination of these drugs showed excellent cancer cell killing capability rather than the drugs alone. The IC<sub>50</sub> of NFER nanodrug in PC12 cells were further evaluated, which can be detected at the concentration of 0.24 mg/mL (Fig. 6B). Another cancer cell line 4T1 was used for cytotoxicity evaluation.

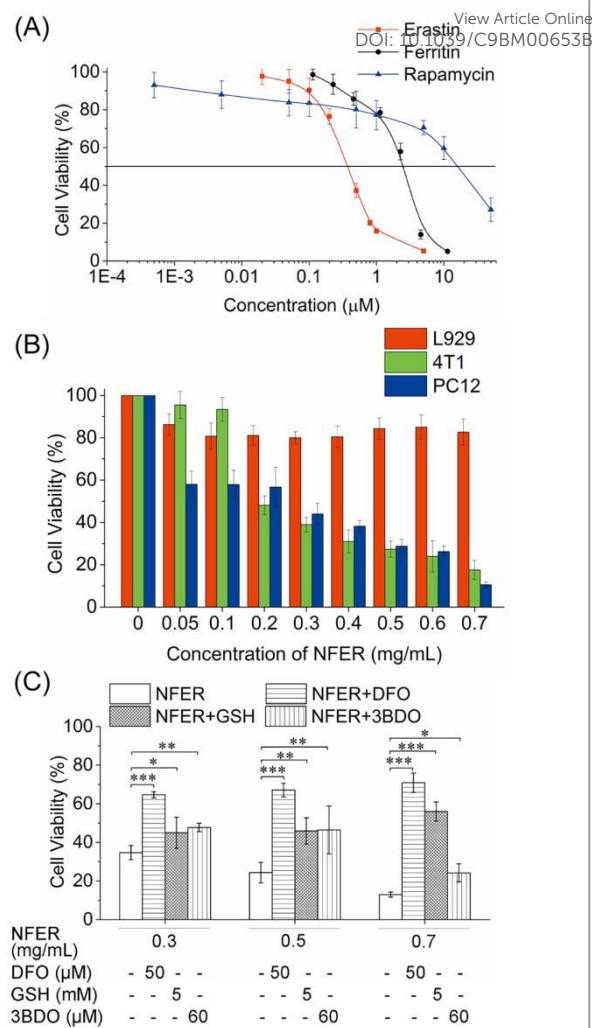
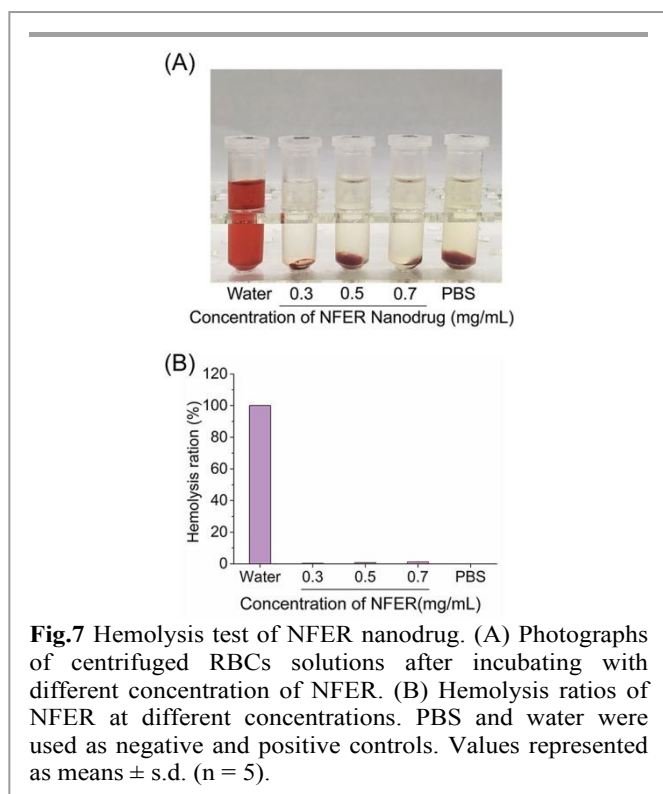


**Fig.6** (A) In vitro cytotoxicity of ferritin, rapamycin, and erastin in PC12 cells for 24 h. (B) In vitro cytotoxicity of NFER in L929, 4T1, and PC12 cells for 24 h. (C) In vitro cytotoxicity of NFER in PC12 cells for 24 h in the presence of ferroptosis and autophagy inhibitors, including DFO (50  $\mu$ M), GSH (5 mM), and 3BDO (60  $\mu$ M). Values represented as means  $\pm$  s.d. (n = 5). Student's t test. \*p < 0.05, \*\*p < 0.01, \*\*\*p < 0.001.

The IC<sub>50</sub> of NFER nanodrug in 4T1 cells was similar with that in PC12 cells. These results suggest that NFER got a significantly increasing cytotoxicity compared with that of ferritin.

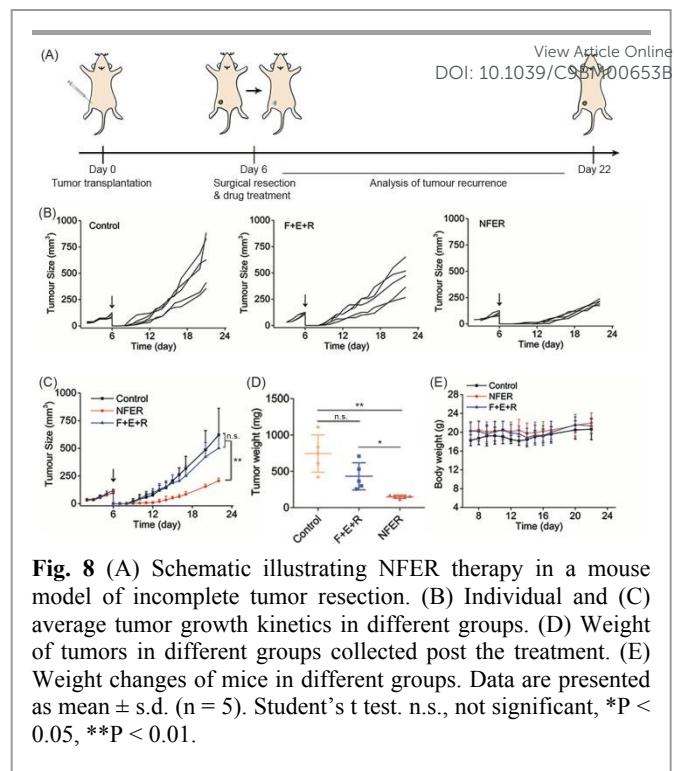
Furthermore, to investigate whether the cytotoxicity of NFER is induced by ferroptosis, the PC12 cells were treated with several inhibitors for different signal pathway together with NFER treatment. Desferrioxamine (DFO) is a medication that binds iron and aluminium, is specifically used in iron overdose, hemochromatosis either due to multiple blood transfusions or an underlying genetic condition, and aluminium toxicity in people on dialysis.<sup>49</sup> The ferroptosis process can be inhibited by DFO because of the iron-chelating property.<sup>50</sup> As shown in Fig. 6C, the cytotoxicity of NFER can be significantly reduced after 50  $\mu$ M DFO treatment. The cell viability of PC12 cells treated with 0.7 mg/mL NFER increased from 12.9% to 70.9% after DFO treatment. The results suggest that the iron in NFER is extremely important for inducing ferroptosis. As



reducing agent glutathione (GSH) depletion induced ferroptosis by erastin treatment in cells was reported,<sup>2</sup> extra GSH treatment can also inhibit ferroptosis. The cell viability of PC12 cells treated with 0.7 mg/mL NFER increased from 12.9% to 56.0% after 5 mM GSH treatment, which verified the ferroptosis-induced cytotoxicity of NFER. As the autophagy-induced ferritin degradation demonstrated by western blot, the autophagy inhibitor should also have effect on reducing the cytotoxicity of NFER. As shown in **Fig. 6C**, the autophagy inhibitor 3BDO can significantly reduce the cytotoxicity of NFER, which means that the cytotoxicity of NFER is also owing to the autophagy process. Taken together, these results suggest that the cytotoxicity is attributed by the autophagy-associated ferroptosis which was induced by NFER nanodrug.

**Biocompatibility of NFER nanodrug.** The hemolytic activity of NFER nanodrug was evaluated by hemolysis assay. Photographs of centrifuged RBCs solutions and hemolysis ratios were shown in **Fig. 7**. It can be seen that even 0.7 mg/mL NFER showed very low hemolytic toxicity (< 2%) to red blood cells, which indicated that NFER nanodrug is biocompatible for the usage as an intravenous injectable drug. Moreover, the cytotoxicity of NFER in normal cell line L929 was studied. As shown in **Fig. 6B**, the NFER killed less than 20% of L929 cells while more than 80% of cancer cells were killed with 0.7 mg/mL NFER treated for 24 h. These results reveal the selectively cancer cell killing ability of NFER nanodrug.

**In vivo inhibition of tumor recurrence by NFER nanodrug.** To validate the in vivo anticancer effects of NFER nanodrug, we used an incomplete tumour resection model. Both of the NFER nanodrug and mixed free drugs were encapsulated into a thermo-responsive F-127 hydrogel which can be transformed from sol to gel in vivo<sup>51</sup>. After the surgical resection of tumors, the hydrogel contained drugs were injected into the tumor resection cavity following with analysis of tumor recurrence (**Fig. 8A**). The tumor recurred rapidly over 16



days after surgical resection of tumors without further drug treatment. In contrast, NFER nanodrug showed improved control of tumor regrowth as both tumor size and tumor weight are significantly decreased after treatment (**Fig. 8B, 8C, 8D** and **Fig. S5**). However, the free drugs mixed together did not show obvious control of tumor regrowth compared with control group. The weight of mice did not impacted by treatment revealed that NFER did not have the significant side effects to mice (**Fig. 8E**). All these results demonstrated the significant benefit of utilizing NFER nanodrug in the 4T1 tumor resection model which attributed by the effects of autophagy-associated ferroptosis.

## Conclusions

In summary, as ferroptosis recently highlighted with clinical significance for anticancer treatments, we successfully developed a novel nanodrug based on ferritin, rapamycin and erastin for ferroptosis-associated anticancer therapy. This Abraxane-inspired NFER nanodrug showed uniform size and controllable drug loading ratios. The autophagy-mediated ferroptosis induction process by NFER was proved by fluorescent sensor and western blot. Furthermore, both autophagy and ferroptosis process can be inhibited by the specific inhibitors. Thus, the ferroptosis-based anticancer capability was verified both in vitro and in vivo. The biocompatibility was demonstrated by extremely low hemolysis property and selectively cancer cells killing ability of NFER. Under this exploration, this carrier-free nanodrug based on autophagy-associated ferroptosis mechanism provides a new perspective for cancer treatment.

## Conflicts of interest

There are no conflicts to declare.

## Acknowledgements

Financial support was from the National Natural Science Foundation of China (31671035, 51803082), the National Significant New Drugs Creation Program (2017ZX09304021), the Jiangsu Province Foundation (BK20170204, BK20161137), the Jiangsu Provincial Medical Innovation Team (CXTDA2017024), the Jiangsu Provincial Commission of Health and Family Planning Foundation (LGY2017088, QNRC2016628, H2018069), Wuxi Science and Technology Development Foundation (WX18IIAN046) the Jiangsu Provincial Key Medical Discipline (ZDXKA2016017), and the Innovation Capacity Development Plan of Jiangsu Province (BM2018023).

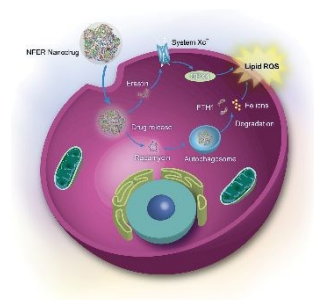
## Notes and references

- L. Ouyang, Z. Shi, S. Zhao, F. T. Wang, T. T. Zhou, B. Liu and J. K. Bao, *Cell Prolif.*, 2012, **90**, 487-498.
- W. S. Yang, R. Sriramaratnam, M. Welsch, K. Shimada, R. Skouta, V. Viswanathan, J. Cheah, P. Clemons, A. Shamji and C. Clish, *Cell*, 2014, **156**, 317-331.
- R. W. Johnstone, A. A. Ruefli and S. W. Lowe, *Cell*, 2002, **108**, 153-164.
- H. Cairtriona, V. S. Sandra, D. B. Longley and P. G. Johnston, *Nat. Rev. Cancer*, 2013, **13**, 714-726.
- S. J. Dixon, K. M. Lemberg, M. R. Lamprecht, S. Rachid, E. M. Zaitsev, C. E. Gleason, D. N. Patel, A. J. Bauer, A. M. Cantley and Y. Wan Seok, *Cell*, 2012, **149**, 1060-1072.
- Z. Shen, J. Song, B. C. Yung, Z. Zhou, A. Wu and X. Chen, *Adv. Mater.*, 2018, **30**, e1704007.
- H. Chen, Z. Gu, H. An, C. Chen, J. Chen, R. Cui, S. Chen, W. Chen, X. Chen, X. Chen, Z. Chen, B. Ding, Q. Dong, Q. Fan, T. Fu, D. Hou, Q. Jiang, H. Ke, X. Jiang, G. Liu, S. Li, T. Li, Z. Liu, G. Nie, M. Ovais, D. Pang, N. Qiu, Y. Shen, H. Tian, C. Wang, H. Wang, Z. Wang, H. Xu, J.-F. Xu, X. Yang, S. Zhu, X. Zheng, X. Zhang, Y. Zhao, W. Tan, X. Zhang and Y. Zhao, *Sci. China Chem.*, 2019, DOI: 10.1007/s11426-018-9397-5.
- S. Zanganeh, G. Hutter, R. Spitler, O. Lenkov, M. Mahmoudi, A. Shaw, J. S. Pajarinen, H. Nejadnik, S. Goodman and M. Moseley, *Nat. Nanotechnol.*, 2016, **11**, 986-994.
- P. Ma, H. Xiao, C. Yu, J. Liu, Z. Cheng, H. Song, X. Zhang, C. Li, J. Wang and Z. Gu, *Nano Lett.*, 2017, **17**, 928.
- C. Zhang, W. Bu, D. Ni, S. Zhang, Q. Li, Z. Yao, J. Zhang, H. Yao, Z. Wang and J. Shi, *Angew. Chem. Int. Ed. Engl.*, 2016, **128**, 2141-2146.
- D.-W. Zheng, Q. Lei, J.-Y. Zhu, J.-X. Fan, C.-X. Li, C. Li, Z. Xu, S.-X. Cheng and X.-Z. Zhang, *Nano Lett.*, 2017, **17**, 284-291.
- T. Liu, W. Liu, M. Zhang, W. Yu, F. Gao, C. Li, S.-B. Wang, J. Feng and X.-Z. Zhang, *ACS Nano*, 2018, DOI: 10.1021/acsnano.8b05860.
- Z. Shen, T. Liu, Y. Li, J. Lau, Z. Yang, W. Fan, Z. Zhou, C. Shi, C. Ke, V. I. Bregadze, S. K. Mandal, Y. Liu, Z. Li, T. Xue, G. Zhu, J. Munasinghe, G. Niu, A. Wu and X. Chen, *ACS Nano*, 2018, **12**, 11355-11365.
- L. Yue, J. Wang, Z. Dai, Z. Hu, C. Xue, Y. Qi, X. Zheng and D. Yu, *Bioconjug. Chem.*, 2017, **28**.
- K. Tino, L. Alan, V. Z. Thomas and U. T. Brunk, *Biochem. J.*, 2004, **378**, 1039-1045.
- G. Huang, H. Chen, Y. Dong, X. Luo, H. Yu, Z. Moore, B. Erik A., B. David A. and J. Gao, *Theranostics*, 2013, **3**, 116-126.
- F. Kratz, *J. Control. Release*, 2008, **132**, 171-183.
- W. Lohcharoenkal, L. Y. Wang, Y. C. Chen and Y. Rojanasakul, *BioMed Res. Int.*, 2014, **2014**, 180549.
- A. Maham, Z. Tang, H. Wu, J. Wang and Y. Lin, *Small*, 2010, **5**, 1706-1721.
- F. Kratz, *J. Control. Release*, 2014, **190**, 331-336.
- M. Liang, K. Fan, M. Zhou, D. Duan, J. Zheng, D. Yang, J. Feng and X. Yan, *Proc. Natl. Acad. Sci. U. S. A.*, 2014, **111**, 14900-14905.
- Z. Zhen, W. Tang, H. Chen, X. Lin, T. Todd, G. Wang, T. Cowger, X. Chen and J. Xie, *ACS Nano*, 2013, **7**, 4830.
- M. M. Abd Elwakil, M. T. Mabrouk, M. W. Helmy, E. A. Abdelfattah, S. K. Khiste, K. A. Elkhodairy and A. O. Elzoghby, *Nanomedicine (Lond)*, 2018, **13**, 2015-2035.
- B. Mao, C. Liu, W. Zheng, X. Li, R. Ge, H. Shen, X. Guo, Q. Lian, X. Shen and C. Li, *Biomaterials*, 2018, **161**, 306-320.
- C. M. Dawidczyk, C. Kim, J. H. Park, L. M. Russell, K. H. Lee, M. G. Pomper and P. C. Searson, *J. Control. Release*, 2014, **187**, 133-144.
- Q. Chen, C. Liang, C. Wang and Z. Liu, *Adv. Mater.*, 2015, **27**, 903.
- N. Serna, L. Sánchez-García, U. Unzueta, R. Díaz, E. Vázquez, R. Mangués and A. Villaverde, *Trends Biotechnol.*, 2018, **36**, 318.
- K. Orino and K. Watanabe, *Vet. J.*, 2008, **178**, 191-201.
- M. A. Siimes, J. E. Addiego and P. R. Dallman, *Blood*, 1974, **43**, 581-590.
- K. Fan, C. Cao, Y. Pan, D. Lu, D. Yang, J. Feng, L. Song, M. Liang and X. Yan, *Nat. Nanotechnol.*, 2012, **7**, 459.
- M. Yang, Q. Fan, R. Zhang, K. Cheng, J. Yan, D. Pan, X. Ma, A. Lu and Z. Cheng, *Biomaterials*, 2015, **69**, 30-37.
- W. Hou, Y. Xie, X. Song, X. Sun, M. T. Lotze, R. Kang and D. Tang, *Autophagy*, 2016, **12**, 1425-1428.
- M. Gao, P. Monian, Q. Pan, W. Zhang, J. Xiang and X. Jiang, *Cell Res.*, 2016, **26**, 1021.
- K. D J and E. S D, *Science*, 2000, **290**, 1717-1721.
- R. Skouta, M. Hayano, K. Shimada and B. R. Stockwell, *Bioorg. Med. Chem. Lett.*, 2012, **22**, 5707-5713.
- Y. Yu, Y. Xie, L. Cao, L. Yang, M. Yang, M. T. Lotze, H. J. Zeh, R. Kang and D. Tang, *Mol. Cell. Oncol.*, 2015, **2**, -.
- J. J. Augustine, K. A. Bodziak and D. E. Hricik, *Drugs*, 2007, **67**, 369-391.
- S. S, R. B, F. R A and R. D C, *Cell Death Differ.*, 2009, **16**, 46-56.

39. G. Di, H. Lei, H. Shuya, P. Nan, W. Pengchong, J. Zheng, Z. Jing, S. Le, Z. Shangli and Z. Yun, *Autophagy*, 2014, **10**, 957-971.
40. X. Wang, J. Yan, D. Pan, R. Yang, L. Wang, Y. Xu, J. Sheng, Y. Yue, Q. Huang and Y. Wang, *Adv. Healthc. Mater.*, 2018, e1701505.
41. Q. Chen, C. Wang, X. Zhang, G. Chen, Q. Hu, H. Li, J. Wang, D. Wen, Y. Zhang, Y. Lu, G. Yang, C. Jiang, J. Wang, G. Dotti and Z. Gu, *Nat. Nanotechnol.*, 2019, **14**, 89-97.
42. J. Wu, M. Shi, W. Li, L. Zhao, Z. Wang, X. Yan, W. Norde and Y. Li, *Colloids Surf. B Biointerfaces*, 2015, **127**, 96-104.
43. S. Y. Wan and B. R. Stockwell, *Trends Cell Biol.*, 2016, **26**, 165-176.
44. G. O. Latunde-Dada, *Biochim. Biophys. Acta*, 2017, **1861**, 1893.
45. Y. Nicholas, v. R. Moritz, Z. Elma, B. Andras J, Y. Wan Seok, F. Daniel J, W. Adam J, S. Inese, P. John M and B. J Jay, *Nature*, 2007, **447**, 864-868.
46. G. Kroemer and M. Jäättelä, *Nat. Rev. Cancer*, 2005, **5**, 886.
47. A. Kuma, M. Matsui and N. Mizushima, *Autophagy*, 2007, **3**, 323-328.
48. Z. Zhou, Y. Yan, K. Hu, Y. Zou, Y. Li, R. Ma, Q. Zhang and Y. Cheng, *Biomaterials*, 2017, **141**, 116-124.
49. M. C. Stuart, M. Kouimtzi and S. Hill, *WHO Model Formulary 2008*, 2009.
50. A. Bruni, A. R. Pepper, R. L. Pawlick, B. Gala-Lopez, A. F. Gamble, T. Kin, K. Seeberger, G. S. Korbitt, S. R. Bornstein, A. Linkermann and A. M. J. Shapiro, *Cell Death Dis.*, 2018, **9**, 595.
51. Y. Liu, W.-L. Lu, J.-C. Wang, X. Zhang, H. Zhang, X.-Q. Wang, T.-Y. Zhou and Q. Zhang, *J. Control. Release*, 2007, **117**, 387-395.

View Article Online  
DOI: 10.1039/C9BM00653B

## Table of contents



Intracellular autophagy-mediated ferroptosis induction process by NFER nanodrug which was assembled by ferritin, erastin, and rapamycin.